JOURNAL OF SCIENCE AND TECHNOLOGY
ISSN: 2229-8460 e-ISSN: 2600-7924

JST

Vol. 17 No. 1 (2025) 71-84
https://publisher.uthm.edu.my/ojs/index.php/jst

I-V Characteristics of GaAs/AlAs Asymmetric Spacer Layer Tunnel Diode (ASPAT) Using Statistical Validation

E. Jamil[1], N. A. AzizulRahman[1], M. Othman[1], S. A. Rahman[1], W. Z. Wan Ismail[1], K. N. Z. Ariffin[1]*

[1] *Faculty of Engineering and Built Environment*
Universiti Sains Islam Malaysia, Bandar Baru Nilai, 71800, MALAYSIA

*Corresponding Author: nabilahzainul@usim.edu.my
DOI: https://doi.org/10.30880/jst.2025.17.01.008

Article Info

Received: 28 November 2024
Accepted: 11 June 2025
Available online: 30 June 2025

Keywords

Statistical validation, slope and intercept hypothesis test, asymmetric spacer layer tunnel diode, linear regression, non-linear regression

Abstract

The Asymmetric Spacer Layer Tunnel Diode (ASPAT) has been physically fabricated and simulated using (2) Silvaco Atlas, a widely used semiconductor device simulation software. The ASPAT features an asymmetrical structure, leading to asymmetric current-voltage (I-V) characteristics, making it suitable as a zero-bias detector with low power consumption for high-frequency applications. Accurately validating these characteristics is critical to assessing the device's performance. However, existing numerical models rely on the Poisson, Schrödinger, and Tsu-Esaki equations, which only account for tunnelling behaviour in discrete regions emitter, barrier, and collector without fully incorporating the effects of doping concentration, material composition, and interface defects. The Transfer Matrix Method (TMM), while addressing some limitations, assumes perfect interfaces, which may not always be the case in three-dimensional (3D) fabricated devices. This study aims to investigate the numerical models used for ASPAT diode design, identify their limitations, propose an improved numerical model, and validate the proposed model against existing methods. The fabrication process of the ASPAT diode involves molecular beam epitaxy (MBE) for the Gallium Arsenide/Aluminum Arsenide (GaAs/AlAs) structure, followed by metal contact deposition, with detailed consideration of doping concentrations and potential material mismatches at the interfaces. Statistical validation of experimental and simulated I-V characteristics is conducted using linear regression, non-linear regression, and hypothesis testing of slope and intercept coefficients. (1) To ensure accuracy, a 5% significance level is assumed for validation. Results indicate that the experimental and simulation data align within a justified 5% error margin, confirming ≥ 95% validation accuracy to confirm the perfect validation despite of several limitations in physical simulation. However, the impact of 3D structural effects, boundary defects, and thermal influences must be further examined to enhance ASPAT performance. This study provides a refined numerical approach to improving ASPAT diode characterization for optimized design and performance evaluation.

1. Introduction

The rising demand for dependable and efficient electronic devices that function at elevated temperatures and terahertz (THz) frequencies has propelled the advancement of novel semiconductor technologies [1][2]. Terahertz technology occupies a distinctive place in the electromagnetic spectrum and is essential for applications including high-speed wireless communication, imaging, spectroscopy, sensing, and security systems [3]. High congestion in the radio spectrum due to the massive number of wireless communication devices has led to significant lag in industries where communication is a major operation [4][5][6][7]. The Terahertz band is envisioned to resolve the current speed scarcity and capacity limitations of the spectrum by enabling Tbps wireless links [8][9]. However, research on Terahertz applications in communication systems is still in its infancy due to high costs and the lack of devices such as oscillators and receivers that can operate across a wide range of temperatures [10][11][12]. Research into terahertz (THz) applications for communication systems offers substantial potential for enabling ultra-fast, high-capacity wireless networks, but significant technical and economic challenges currently impede its advancement [13][14]. The Asymmetric Spacer Layer Tunnel (ASPAT) diode, developed by R.T. Syme and colleagues in 1990, marked a notable breakthrough in terahertz (THz) technology, particularly due to its superior temperature stability [15]. Its innovative design enables reliable operation over a broad temperature range, making it highly suitable for THz applications. Unlike Schottky and Ge backward diodes, which typically require low temperatures to perform optimally, the ASPAT diode delivers consistent performance without the need for cooling [16][17]. When incorporated into resonant tunneling diode (RTD) technology, ASPAT has achieved impressive data rates of up to 56 Gb/s, highlighting its promise for high-speed wireless communication [18][19]. In 2018, K.N.Z. Ariffin presented a [Q3]3-D physical model of the ASPAT diode that was validated against experimental data in terms of DC performance [20]. A 3-D model of the ASPAT device, previously designed in Silvaco, presents physical design and graphical observations in Figure 2(a) and Figure 2(b). These observations indicate that the simulation of the device's DC performance was excellently validated against the experimental data, as evidenced by the overlap between the simulated and experimental graphs.

However, the study did not include a conclusion on the percentage of validation between the two datasets or define a significant interval for the acceptance of current-voltage characteristic data. By confirming the significant interval and the validation percentage between both datasets, the precision of the I-V characteristics can be enhanced. The precision of the ASPAT diode's I-V characteristics is crucial for microwave small signal analyses, including voltage sensitivity, tangential sensitivity, and dynamic range. The validation process uses a 5% error margin or a 95% confidence interval from experimental results through regression and hypothesis testing [21], [22]. The simulation of I-V characteristics should fall within this significant interval, as illustrated in Fig. 1.

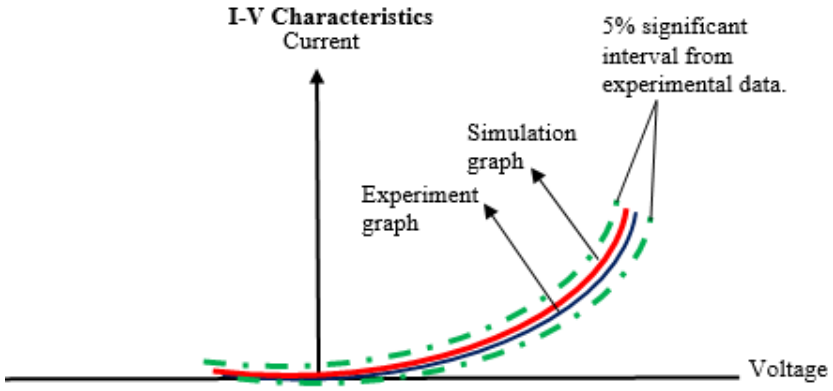

Fig. 1 *The illustration for I-V characteristics precision for ASPAT simulation based on 5% error or 95% significant interval of experimental data*

2. Methodology

Fig. 2 presents the exponential graphs for both the experimental and simulated current-voltage characteristics of the ASPAT diode, based on a previous study conducted by K.N.Z. Ariffin. The simulation data was generated using Silvaco Atlas, a widely used semiconductor device simulation software. In this statistical validation, the exponential equations representing both graphs are converted into linear equations. The parameters obtained from the linear regression will then be used as initial estimated values in a non-linear regression analysis using Minitab. At this stage, Minitab will mathematically refine the initial estimates and converge toward the actual curve. Finally, a hypothesis test will be conducted to determine the validation percentage for the slope and intercept between the two graphs.

J. of Science and Technology Vol. 17 No. 1 (2025) 71-84

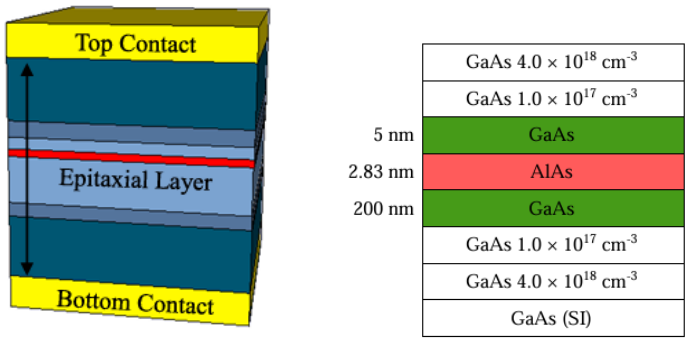

Fig. 2 (a) *A 3-D model of GaAs AlAs ASPAT with epitaxial layers designed in Silvaco (Q6)*

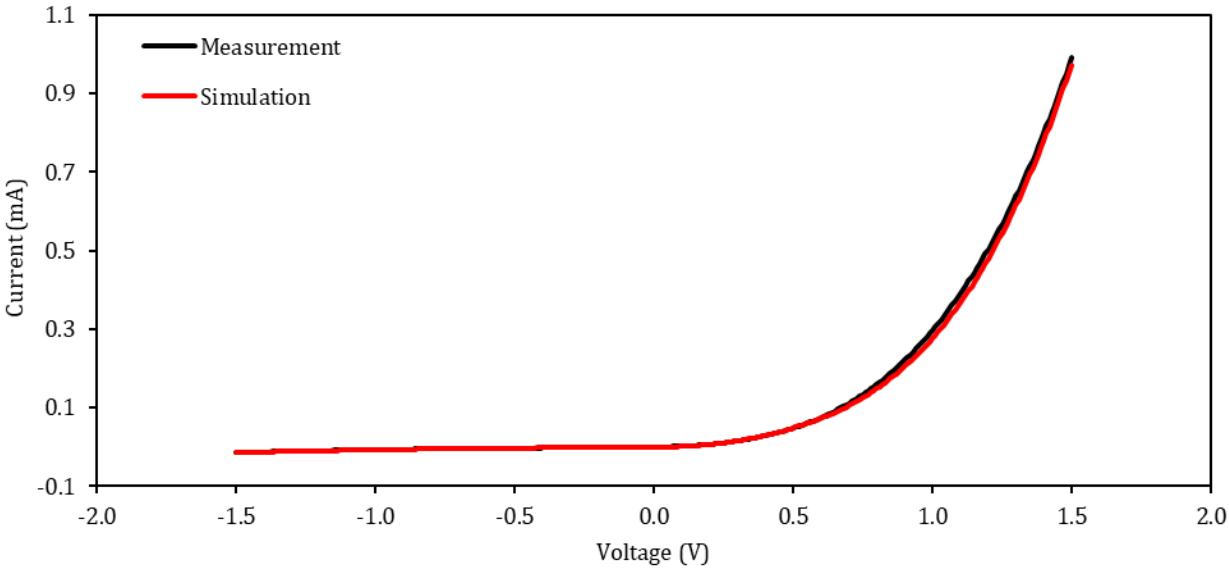

Fig. 3 (b) *Current-voltage characteristics of ASPAT for experiment and simulation data*

2.1 Linear Regression

The statistical validation of ASPAT begins with the development of a linear regression model that fits the experimental and simulation graphs. The purpose of the regression model is to develop a mathematical equation that represents the linear relationship between voltage and current using a statistical approach [23][24]and to determine the initial values that will be used in non-linear regression. This validation will implement a simple linear regression, as it involves one predictor (voltage) and one response (current) [25]. The linear regression will be modeled as an exponential equation since the I-V characteristics follow an exponential curve, as shown in Eq. 1 and Fig. 2. The exponential equation will then be converted to a linear equation, as illustrated from Equation 1—Equation 8.

$$y = ae^{bx} + \mathcal{E} \tag{1}$$

In Eq. 1, y represents the current, a and b are constants, x is the voltage value, and ε represents the independent error terms that follow a normal distribution with a mean of zero. Adding a natural log to both sides of Eq. 1 results in Eq. 2 and 3:

$$ln\, y = ln(a) + \ln(e^{bx}) \tag{2}$$

$$ln\, y = ln(a) + bx \tag{3}$$

Eq. 3, when compared with the general linear equation $z = a_o + a_1 x$ results in Equations 4 to 6.

$$z = ln\, y \; ; a_o = ln\, a \; ; \; a_1 = b \tag{4}$$

$$ln\, y = ln(a) + bx \tag{5}$$

$$a = e^{ao}, b = a_1 \tag{6}$$

Using the linear regression model formula, a_0 and a_1 can be calculated as shown in Equations 7 and 8.

$$a_1 = \frac{n\sum_{i=1}^{n} x_i\, z_i - \sum_{i=1}^{n} x_i \sum_{i=1}^{n} z_i}{n\sum_{i=1}^{n} {x_i}^2 - (\sum_{i=1}^{n} x_i)^2} \tag{7}$$

$$a_0 = \bar{z} - a_1\bar{x} \tag{8}$$

The constants a_0 and a_1 can alternatively be calculated using Minitab. The real value for a can be determined using the formula $a = e^{ao}$ while b is directly taken from a_1 since $b = a_1$. From here, the parameters a and b involved in the exponential equation of the nonlinear I-V characteristics $y = ae^{bx}$ can be adopted as initial parameters in the non-linear statistical analysis using Minitab. The prediction for a_1 and a_0 can be obtained in Minitab Software by navigating to **Stats > Regression > Fitted Line Plot**. By choosing a 'Linear Model' to achieve a linear equation, set the 'Response (Y)' to *'ln(abs(current))'* and the 'Predictor (*X*)' to '*Voltage'* value. Minitab will then generate the linear equation $z = a_o + a_1x$. Hence, the exponential equation $y = ae^{bx}$ can be derived from Equations 9 to 12.

$$z = a_o + a_1x \tag{9}$$

$$a = e^{ao}, b = a_1 \tag{10}$$

$$y = ae^{bx} \tag{11}$$

$$y = ae^{bx} \tag{12}$$

From Equation 9 to Equation 12, both the linear and exponential equations are derived through the transformation of equations. The exponential equation involving e^{a0} and a_1 (Eq. 12) becomes the initial parameters that will be estimated in the non-linear regression analysis. However, before this equation is adopted in non-linear regression, several analyses need to be conducted to determine if the association between the response (current) and predictor (voltage) in the model is statistically significant. The R^2 value, or the coefficient of determination, is an indicator used to assess the goodness of fit for the data to the regression line. It ranges between 0 (0%) and 1 (100%), with a value closer to 1 indicating that the data closely fits the regression line, while a lower value suggests a poorer fit. The P-value interprets the significance of the slope and intercept coefficients. If the P-value is less than 0.05, we can conclude that the coefficients provide a better fit, indicating that they are significant for the regression line. Otherwise, the coefficients are not considered the best estimate for the regression line. Lastly, the line of regression is assessed through the linear regression equation $z = a_o + a_1x$ to test the slope and intercept hypothesis.

2.2 Non-Linear Regression

From Eq. 12, the non-linear regression model was fitted in Minitab as $\mathbf{y = e^{a0}e^{a1x}}$. First, select Stat > Regression > Nonlinear Regression with the exponential function *Theta1*e^(Theta2*x)*. Choose '*Voltage'* as the Actual Predictor, 'Current' as the Response, and for the Parameters, set *Theta1* as $\boldsymbol{e^{a0}}$ and *Theta2* as a_1. By default, Minitab implements the Gauss-Newton method to determine the least squares estimation for the non-linear model. This method uses a linear approximation to the expectation function to iteratively improve the initial coefficients, continually refining the estimates until the relative offset falls below the prescribed tolerance [26]. Several outputs were selected to be displayed in the non-linear regression analysis, such as the mean response plot (predicted current) calculated from the regression equation, regression standard error, the exponential non-linear equation, and standard error for the exponential coefficient.

2.3 Hypothesis Testing on the Slope and Intercept of Regression Line for Validation of Experiment and Simulation DC Performance

The regression line that interprets the relationship between the current-voltage characteristics of the experimental and simulation data needs to be validated through hypothesis testing. This procedure requires

J. of Science and Technology Vol. 17 No. 1 (2025) 71-84

additional analysis of the regression model. It is essential that the model residual errors, e_i, normally distributed, or that the mean of the errors remains zero with a certain variance [22], [24]. When the meaning of the residual errors is zero, it indicates that the slope of the regression line is the ideal slope that accurately represents the relationship depicted in the graph. For instance, if we have a set of *x* and *y* data, the mean is exactly zero when the line of the graph is precisely centered between the scatter of the data, as shown in Fig. 2. Hence, the error is normally distributed.

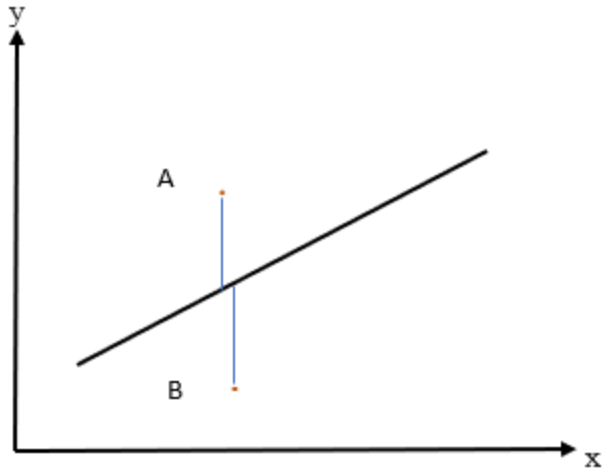

Fig. 4 *Linear regression with equal distribution of error*

Based on Eq. 11 and Fig. 3, if the residual error at point A is 5, then the residual error at point B needs to be -5 so that the residuals are equally distributed.

$$\sum_{i=1}^{n}(y_1 - \hat{y}_1) = \sum_{i=1}^{n} e_i = 0 \tag{13}$$

The validation process between simulation and experimental data continues with a hypothesis test on the slope and intercept of the regression line. The goal of this hypothesis test is to determine whether the slope and intercept of the simulation are validated against the experiment within a 5% error margin, which is commonly adopted in many validation cases [4]. If the slope and intercept coefficients of the simulation fall within a 5% range at the upper and lower tails of the experimental slope, then the simulation data is validated. In some cases, achieving zero mean error is challenging due to factors such as data scatter. Therefore, it is necessary to test the means of residual errors before conducting hypothesis testing on the intercept and slope coefficients. The validation for two regression slopes and intercepts will continue with the hypothesis statements [15] .

First, the null hypothesis is decided as H_o: $b_1 = b_2$. Here, b_1 is the regression slope for the simulation, and b_2 is the regression slope for the experimental data. The hypothesis indicates that the slope of the simulation is exactly similar to the slope of the experimental data. The alternative hypothesis is H_1: $b_1 \neq b_2$, which indicates that the slope of the simulation is different from the experiment. From both hypotheses, we indicate the rejection criterion is at the lower and upper tails of the normal distribution curve with an alpha of 0.05, or a 5% rejection criterion. This is because the graph for simulation data can be located either below or above the experimental graph. Then, the test statistics need to be determined to test the null hypothesis. Since we have a large sample (each sample > 25), the test statistic will be the normal *z*. This test is computed as the difference between the two slopes of the regression line, b_1 and b_2, divided by the standard error of the difference between the slopes, S_{b1-b2}, denoted as Eq. 14 . The null hypothesis, alternative hypothesis, and *z* test will be repeated with the intercept coefficient of the two regression lines by alternately changing b_1-b_2 to the difference between two intercept coefficients and S_{b1-b2} with the difference of intercepts' standard error between the two regression lines.

$$z = \frac{b_1 - b_2}{s_{b1-b2}} \tag{14}$$

Once the *z* test formula is determined and calculated, it needs to be interpreted using the z-score chart and the normal distribution curve. The z-score chart is used to find the area under a normal distribution curve. Since we decided the rejection area is 5 %, or alpha 0.05, the upper and lower tail areas under the normal distribution curve are 0.025, as shown in Fig. 4. The *z* value calculated from Equation 14 will be considered at the lower (-*z*)

and upper (+z) tail curves. If the area from the calculated z for the upper and lower tails falls within the rejection area, then the null hypothesis is rejected; otherwise, the hypothesis is accepted. Once the hypothesis is accepted, we can conclude that the regression slope and intercept for the simulation and experimental data are validated within a 5 % error margin.

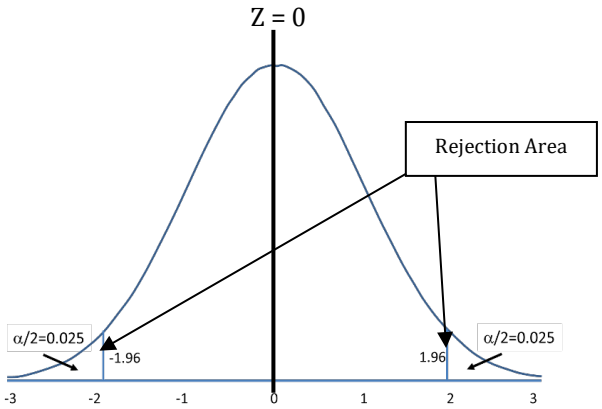

Fig. 5 *Normal distribution curve*

3. Results and Discussion

This section discusses the slope and intercept validation for non-linear I-V characteristics using three assessments: linear regression analysis, non-linear regression analysis, and hypothesis testing. These analyses were conducted using Minitab software. Firstly, the non-linear exponential equation $y = ae^{bx}$ is converted into a linear equation $ln\, y = ln(a) + bx$ as shown in Eq. 3. Based on this equation, linearity is achieved by converting the current data (y axis) into *ln(current)*. Note that negative natural logarithm values cannot be solved, so the current is converted to an absolute value before calculating *ln(current)*. The value of *abs(ln(current))* with respect to voltage is plotted, as shown in Fig. 5.

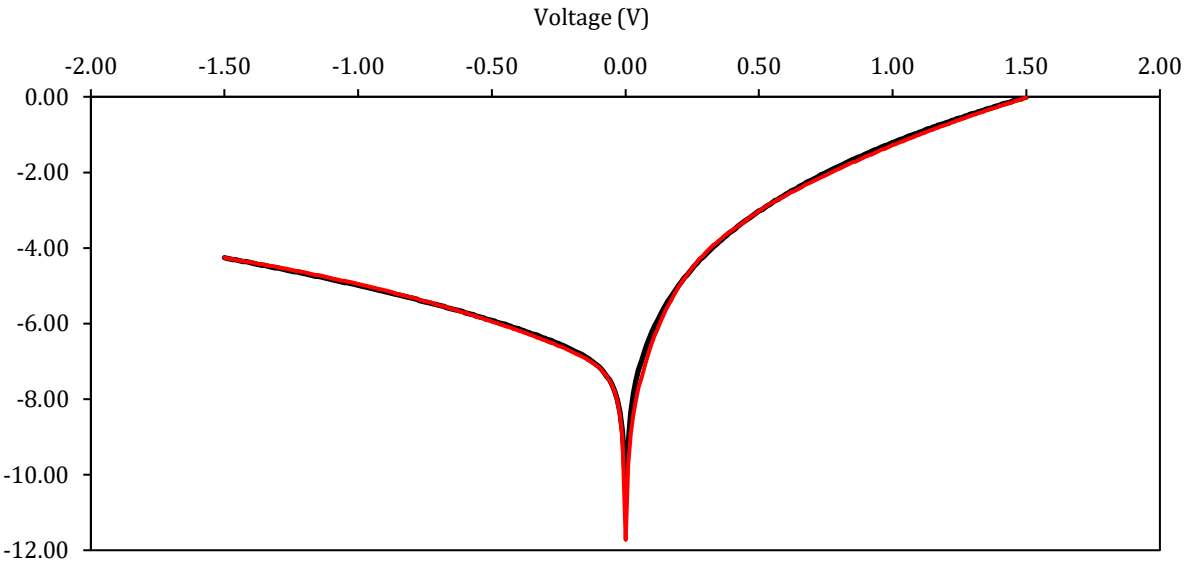

Fig. 6 *The ln (I)-V characteristics of GaAs/AlAs ASPAT*

3.1 Linear Regression Analysis

In Figure 5, there are two slopes, A and B, located on the positive and negative sides of the I-V characteristics, respectively. Thus, the linear regression, non-linear regression, and coefficient hypothesis test will be conducted for sides A and B individually. Through the regression analysis in Minitab, the linear regression lines that fit the graph at sides A and B can be observed in Fig. 6 for the experimental data, while the regression lines that fit the graph at sides A and B for the simulation data can be seen in Fig. 7.

J. of Science and Technology Vol. 17 No. 1 (2025) 71-84

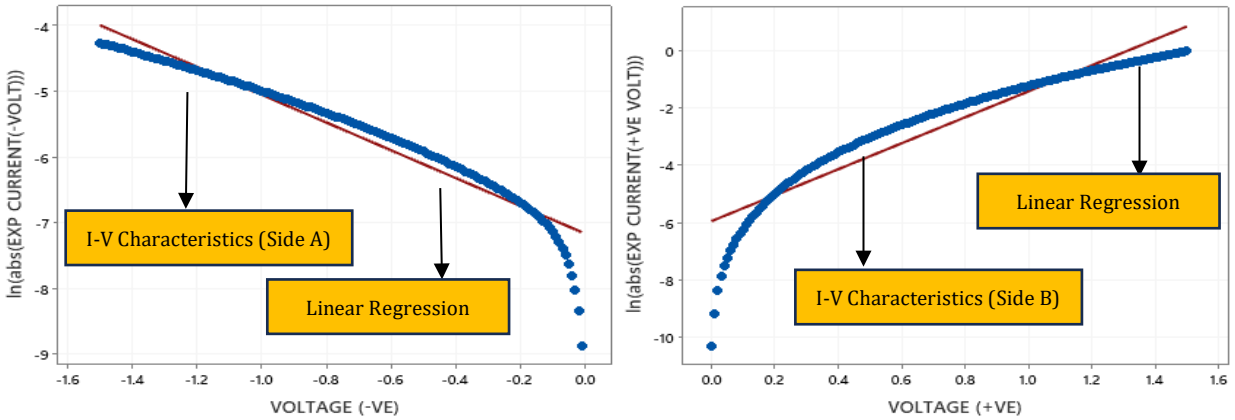

(a) **(b)**

Fig. 7 *The linear regression for experiment data (a) Side A; and (b) Side B*

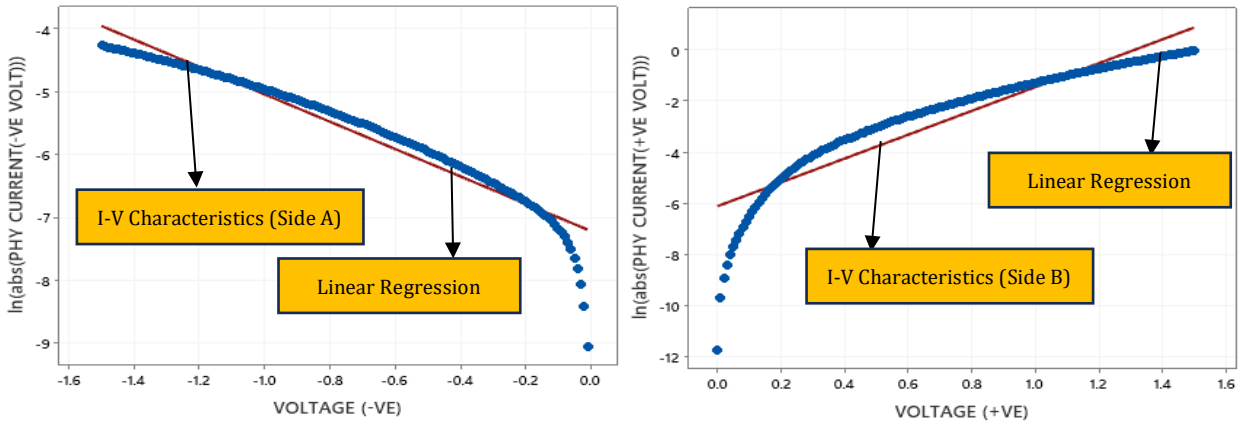

(a) **(b)**

Fig. 8 *The linear regression for simulated data (a) Side A; and and (b) Side B*

The assessment of the goodness of fit of the regression line for all data can be observed in table 1:

Table 1 *Parameters for evaluation the goodness of linear regression*

Regression Analysis	R^2	*P*-Value	Linear Regression Equation $z = a_o + a_1 x$ *ln(current) = ln(a) + b(voltage)* *z = ln(current); a_0 = ln(a); a_1 = b*
Experiment Data (Side A)	93.00 %	0.000	$z = -7.164 - 2.113(x)$
Experiment Data (Side B)	87.75 %	0.000	$z = -5.943 + 4.534(x)$
Simulation Data (Side A)	92.93 %	0.000	$z = -7.214 - 2.175(x)$
Simulation Data (Side B)	84.58 %	0.000	$z = -6.114 + (x)$

Based on Table 1, the linear regression for all slopes can be predicted using the linear regression formula z: $a_o + a_1 x$. The coefficient of determination (R) for the experimental regression lines for sides A and B are 93 % and 87.75%, respectively, while the simulation data for sides A and B are 92.93 % and 84.58 %, respectively. This indicates that the regression lines fit the data excellently. If the coefficient of determination reaches 100 %, it indicates that the residual errors are normally distributed. For these regression lines, all *P*-values are below 0.05, which allows us to conclude that there is a statistically significant association between the response variable and the predictor term.

Overall, all analyses demonstrate that the regression lines significantly interpret the relationship of the I-V characteristics. Therefore, they can be used as initial parameters in non-linear regression analysis.

3.2 Non-Linear Regression Analysis

The non-linear regression was conducted using the Gauss-Newton algorithm, with a maximum of 1000 iterations and a tolerance of 0.00001. The fitted line plots for sides A and B of both the simulation and experiment are shown in Fig. 10 through 13, while the parameters for analyzing the fitness of the regression lines for all data are shown in Table 2.

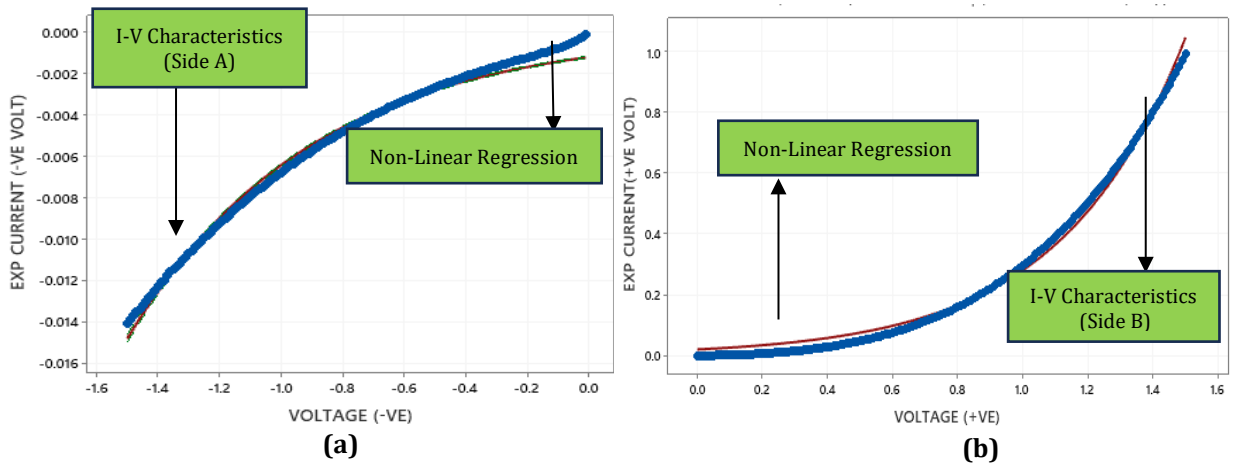

Fig. 9 *Fitted non-linear regression for experimental data (a) Side A; and (b) Side B*

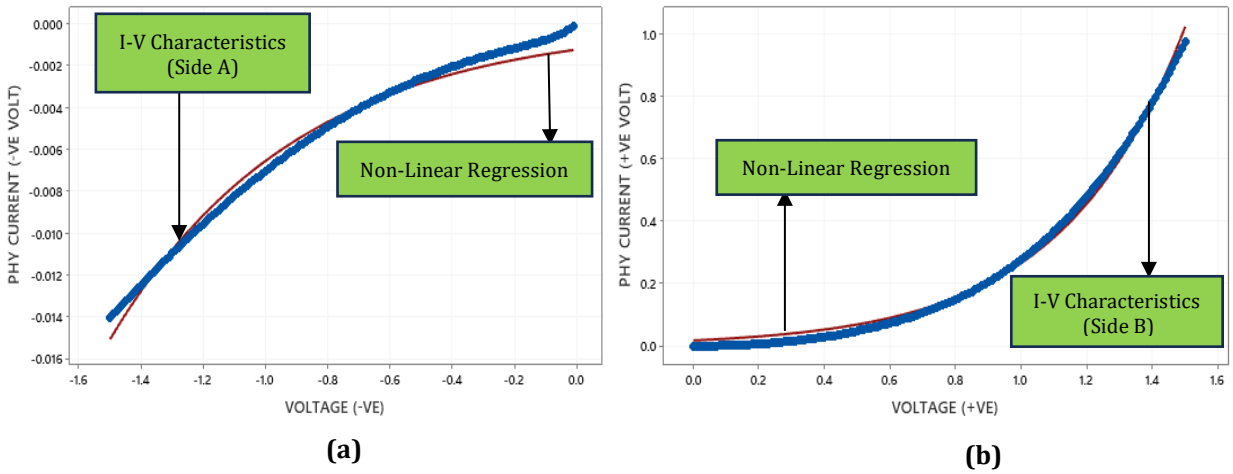

Fig. 10 *Fitted non-linear regression for simulated data (a) Side A; and (b) Side B*

Table 2 *Parameter analysis of non-linear regression model*

Parameters for Analysis	Exponential Equation	Mean of Residual Error
Experiment Data (Side A)	$I = -0.001218e^{(-1.66568V)}$	0.00
Experiment Data (Side B)	$I = 0.020237e^{(2.63093V)}$	0.00
Simulation Data (Side A)	$I = -0.001237e^{(-1.66672V)}$	0.00
Simulation Data (Side B)	$I = 0.017970e^{(2.69475V)}$	0.00

3.3 Validation: Hypothesis Test for Slope, (a_1) and Intercept, (a_0) of $z = a_o + a_1 x$

The hypothesis test for all coefficients is conducted using the z-test and normal distribution graphs. This requires that the residual errors of the non-linear exponential equation be normally distributed. In other words, the mean residual errors should be zero, as shown in Table 2. Non-linear regression generates the exponential relationship

of the I-V characteristics as $\boldsymbol{y = ae^{bx}}$. This exponential equation is transformed into a linear equation, $\boldsymbol{z = a_o + a_1 x}$, for sides A and B respectively, to ensure that the slope and intercept coefficients can be interpreted for hypothesis testing. The linear equation for all exponential equations can be summarized in Table 3.

Table 3 *The linearization of exponential equation*

Equations	Exponential Equations $y = ae^{bx}/I = ae^{b(V)}$	Linear Equations $z = a_o + a_1 x$ $\ln(I) = \ln(a) + b(V)$
Experiment Data (Side A)	$I = -0.001218e^{(-1.66568V)}$	ln(I) = -6.710545 -1.66568(V)
Experiment Data (Side B)	$I = 0.020237e^{(2.63093V)}$	ln(I) = -3.900243 + 2.63093(V)
Simulation Data (Side A)	$I = -0.001237e^{(-1.66672V)}$	ln(I) = -6.695066 – 1.66672(V)
Simulation Data (Side B)	$I = 0.017970e^{(2.69475V)}$	ln(I) = -4.019052 + 2.69475(V)

The slope for experimental data on Side A will be validated against the slope for simulation data on the same side, and the slope for experimental data on Side B will be compared with the slope of simulation data on the same side. This test will be repeated for the intercept coefficients as presented in Tables 4 and 5. Based on Table 4, the null hypothesis for Side A is H_0: $a_{2(\text{slope of simulation})} = -1.66568_{(\text{slope of experiment})}$. This hypothesis indicates that the slope for simulation data on Side A is similar to the slope of experimental data with a value of -1.66568. The alternative hypothesis is H_1: $a_{2(\text{slope of simulation})} \neq -1.66568_{(\text{slope of experiment})}$, which indicates that the slope of simulation and experiment data is not similar (≠ -1.66568). By using an alpha of 0.05, the similarity between the two slopes will be tested within a 5% deviation, meaning the slope for simulation at Side A can only differ from the experimental slope within a 5% error to accept the null hypothesis. The hypothesis test proceeds with the calculation of the z-value. Since the test is two-sided on the normal distribution curve, the z-value will be considered positive and negative, with the rejection area at 0.025 on both sides of the normal distribution curve, as shown in Fig. 4.

$$z = \frac{a_1 - a_2}{s_{a1-a2}} \tag{15}$$

Based on Eq. 15, a_1- a_2 represents the difference between the slopes for experimental and simulation data, while $s_{a1\text{-}a2}$ is the difference in the standard error of the slopes. The values for a_1 and a_2 are -1.66568 and – 1.66672 respectively, while S_{a1} and S_{a2} are ln [0.0165739] = -4.0999 and ln [0.0201411] = -3.9050, resulting in a z-value of -0.5 and 0.5. The P-value for both sides is 0.5 at the lower tail and 0.5 at the upper tail of the normal distribution curve. Since the P-value is greater than 0.025 at both tails, the null hypothesis fails to be rejected. This indicates that the slope for simulation and experiment data are validated within a 5 % deviation or validated within a 95 % confidence interval. The hypothesis test for the slope coefficient on Side A is repeated for Side B. The null hypothesis for Side B is H_0: $a_{2(\text{slope of simulation})} = 2.63093_{(\text{slope of experiment})}$. This hypothesis indicates that the slope for simulation data in Side B is similar to the slope of experimental data with a value of 2.63093. The alternative hypothesis is H_1: $a_{2(\text{slope of simulation})} \neq 2.63093_{(\text{slope of experiment})}$ indicating that the slope of simulation and experiment data are not similar with a value of 2.63093.

By using an alpha of 0.05, the similarity between the two slopes will be tested within a 5 % deviation, meaning the slope for simulation at Side B can only differ from the experimental slope within a 5 % error to accept the null hypothesis. The hypothesis test proceeds with the calculation of the z-value. Since the test is two-sided on the normal distribution curve, the z-value will be considered positive and negative, while the rejection area is 0.025 on both sides, as shown in Fig. 13. The values for a_1 and a_2 are 2.63093 and 2.69475 respectively, while S_{a1} and S_{a2} are ln [0.0267560] =-3.6210 and ln [0.0234058] =-3.7548, resulting in a z-value of -0.48 and 0.48. The P-value for both sides is 0.68 at the upper tail and 0.28 at the lower tail of the normal distribution curve, both of which are greater than 0.025. Thus, the null hypothesis fails to be rejected, and the slope for simulation and experiment data are validated within a 5 % deviation, or the data is validated with 95% confidence.

Table 4 *The procedure for hypothesis test for slope coefficient at Side A and B*

Steps for Hypothesis Test	Slope Hypothesis Test at Side A	Slope Hypothesis Test at Side B
Null Hypothesis	H_0: $a2_{(\text{slope of sim})}$ = -1.66568 $_{(\text{slope of exp})}$.	H_0: $a2_{(\text{slope of sim})}$ = 2.63093 $_{(\text{slope of exp})}$.
Alternative Hypothesis	H_1: $a2_{(\text{slope of sim})}$ ≠ -1.66568 $_{(\text{slope of exp})}$.	H_1: $a2_{(\text{slope of sim})}$ ≠ 2.63093 $_{(\text{slope of exp})}$.
Slope coefficient	Experiment: -1.66568 Simulation: – 1.66672	Experiment = 2.63093 Simulation = 2.69475
Slope Standard Error	Experiment: *ln* (0.0165739) = -4.0999 Simulation: *ln* (0.0201411) = -3.9050	Experiment = *ln* (0.0267560) = -3.6210 Simulation = *ln* (0.0234058) = -3.7548
Z Test $z = \frac{a_1 - a_2}{s_{a1-a2}}$ a_1 = Slope of experiment a_2 = Slope of simulation S_{a1} = Slope standard error (experiment) S_{a2} = Slope standard error (simulation)	z = -5.33×10^{-3} Lower tail = -0.5 Upper tail = 0.5	z = -0.48 Upper tail = 0.48 Lower tail = -0.48
P-Value (> 0.0025) for both tail	Upper tail = 0.5 Lower tail = 0.5	Upper tail: 0.68 Lower tail: 0.28
Conclusion	Since the *P*-value is greater than 0.025 at both tails, the null hypothesis cannot be rejected. Therefore, the slopes for both the experimental and simulation data at Part A are validated within a 5% error, indicating a validation level of ≥ 95%.	Since the p-value is greater than 0.025 at both tails, the null hypothesis cannot be rejected. Thus, the slopes for both the experimental and simulation data at Part B are validated within a 5% error, confirming a validation level of ≥ 95%.

J. of Science and Technology Vol. 17 No. 1 (2025) 71-84

The hypothesis test for the slope coefficient is repeated for the intercept coefficient, as shown in Table 5.

Table 5 *The procedure for hypothesis testing for intercept coefficients at Side A and B*

Steps for Hypothesis Test	Intercept Hypothesis Test at Side A	Intercept Hypothesis Test at Side B
Null Hypothesis	H_0: $a_{2(\text{intercept of sim})}$ = -6.710545$_{(\text{intercept of exp})}$.	H_0: $a_{2(\text{intercept of sim})}$ =-3.900243 $_{(\text{intercept of exp})}$.
Alternative Hypothesis	H_1: $a_{2(\text{intercept of sim})}$ ≠-6.710545 $_{(\text{intercept of exp})}$.	H_1: $a_{2(\text{intercept of sim})}$ ≠-3.900243 $_{(\text{intercept of exp})}$.
Intercept coefficient	Experiment: - 6.710545 Simulation: -6.695066	Experiment: -3.900243 Simulation: -4.019052
Intercept Standard Error	Experiment: *ln* (0.0000251) = -10.5926 Simulation: *ln* (0.0000310) =-10.3815	Experiment: *ln* (0.0007195) = -7.2370 Simulation: *ln* (0.0005605) = -7.4867
Z Test $z = \frac{a_1 - a_2}{s_{a1-a2}}$ a_1 = Intercept of experiment a_2 = Intercept of simulation S_{a1} = Intercept standard error (experiment) S_{a2} = Intercept standard error (simulation)	z = 0.07 Upper tail = 0.07 Lower tail = -0.07	z= 0.48 Upper tail = 0.48 Lower tail =-0.48
P-Value (> 0.0025) for both tail	Upper tail = 0.53 Lower tail = 0.47	Upper tail = 0.68 Lower tail = 0.32
Conclusion	The *P*-value at both tails is greater than 0.025; thus, the null hypothesis fails to be rejected. Hence, the intercept coefficient for the experiment and simulation at part A is validated within a 5% error, meaning both data sets are concluded to achieve ≥ 95% validation.	The *P*-value at both tails is greater than 0.025; thus, the null hypothesis fails to be rejected. Hence, the intercept coefficient for the experiment and simulation at part B is validated within a 5% error, meaning both data sets are concluded to achieve ≥ 95% validation.

Based on Table 5, the null hypothesis for Side A is H_0: $a_{2(\text{intercept of simulation})}$ = -6.710545 $_{(\text{intercept of experiment})}$. This hypothesis indicates that the intercept coefficient for simulation data on Side A is similar to the intercept coefficient of experimental data with a value of −6.710545. The alternative hypothesis is H_1: $a_{2(\text{intercept of simulation})} \neq$ -6.710545 $_{(\text{intercept of experiment})}$, indicating that the intercept coefficient of simulation and experiment data are not similar at the indicated value. By using an alpha of 0.05, the similarity between the two slopes will be tested within a 5 % deviation, meaning the intercept for simulation at Side A can only differ from the experimental slope within a 5 % error to accept the null hypothesis. The hypothesis test proceeds with the calculation of the *z*-value. Since the test is two-sided on the normal distribution curve, the *z*-value will be considered positive and negative, while the rejection area is 0.025 on both sides of the normal distribution curve, as shown in Fig. 4.

Based on Eq. 13, a_1- a_2 represents the difference between the intercepts for experimental and simulation data, while s_{a1-a2} is the difference in the standard error of the intercepts between the experiment and simulation. The values for a_1 and a_2 are -6.710545 and -6.695066 respectively, while S_{a1} and S_{a2} is $\ln(0.0000251) = -10.5926$ and $\ln(0.0000310) = -10.3815$, resulting in a *z*-value of 0.07 and -0.07. The *P*-value for both sides is 0.47 at the lower tail and 0.53 at the upper tail of the normal distribution curve. Since the *P*-value is greater than 0.025 at both tails, the null hypothesis fails to be rejected. This indicates that the intercept for simulation and experiment data is validated within a 5 % deviation or validated within a 95 % confidence interval. A hypothesis test for the interception coefficient on Side A is repeated for Side B.

The null hypothesis for Side B is H_0: $a_{2(\text{intercept of simulation})}$ = -3.900243 $_{(\text{intercept of experiment})}$. This hypothesis indicates that the intercept coefficient for simulation data on Side B is similar to the intercept coefficient of experimental data. The alternative hypothesis is H_1: $a_{2(\text{intercept of simulation})} \neq$ - 3.900243 $_{(\text{intercept of experiment})}$, indicating that the intercept coefficient of simulation and experiment data are not similar. By using an alpha of 0.05, the similarity between the two slopes will be tested within a 5 % deviation, meaning the intercept for simulation at Side B can only differ from the experimental intercept within a 5 % error to accept the null hypothesis. The hypothesis test proceeds with the calculation of the *z*-value. Since the test is two-sided on the normal distribution curve, the *z*-value will be considered positive and negative, while the rejection area is 0.025 on both sides of the normal distribution curve, as shown in Fig. 4. Based on Eq. 15, a_1- a_2 represents the difference between the intercepts for experimental and simulation data, while s_{a1-a2} is the difference in the standard error of the intercepts between the experiment and simulation. The values for a_1 and a_2, are -3.900243 and -4.019052, respectively, while S_{a1} and S_{a2} are $\ln(0.0007195) = -7.2370$ and $\ln(0.0005605) = -7.4867$, respectively. Thus, the *z*-values for both sides are -0.48 and 0.48. The *P*-values for both sides are 0.32 for the lower tail and 0.68 for the upper tail of the normal distribution curve. Since the *P*-values are greater than 0.025 at both tails, the null hypothesis fails to be rejected. This indicates that the intercepts for the simulation and experimental data are validated within a 5 % deviation or validated within a 95% confidence interval.

4. Conclusion

This study successfully validated the I-V characteristics of the GaAs/AlAs Asymmetric Spacer Layer Tunnel Diode (ASPAT) with an error margin within 5%, confirming ≥ 95% accuracy between experimental and simulation data. The validation process integrated three statistical approaches linear regression to estimate the linear equation, non-linear regression to capture the exponential nature of I-V characteristics, and the Gauss-Newton iterative method for parameter refinement. Hypothesis testing confirmed that both slope and intercept coefficients were statistically significant, ensuring reliable model validation. However, key limitations remain in accurately modelling 3D structural effects, boundary defects, and doping-dependent variations, which significantly impact ASPAT performance. Future research should focus on refining numerical models to incorporate 3D structural and thermal effects, investigating the influence of interface defects and Schottky barrier formation on I-V characteristics and expanding validation to include alternative semiconductor compositions and fabrication tolerances. By addressing these challenges, this study provides a robust numerical framework for optimizing ASPAT diode design, enhancing its performance in high-frequency applications.

Acknowledgement

Communication of this research is made possible through the support by Universiti Sains Islam Malaysia.

Conflict of Interest

There is no conflict of interest regarding the publication of the paper.

Author Contribution

The authors confirm contribution to the paper as follows: ***study conception and design:*** *N. A AzizulRahman, E. Jamil, K. N. Z. Ariffin, M. Othman, S. A. Rahman, W. Z. Wan;* ***data collection:*** *E. Jamil, K. N. Z. Ariffin;* ***analysis and interpretation of results:*** *N. A AzizulRahman, E. Jamil, K. N. Z. Ariffin, M. Othman, S. A. Rahman, W. Z. Wan;* ***draft manuscript preparation:*** *N. A AzizulRahman, E. Jamil, K. N. Z. Ariffin, M. Othman, S. A. Rahman, W. Z. Wan. All authors reviewed the results and approved the final version of the manuscript.*

References

[1] I. F. Akyildiz, C. Han, Z. Hu, S. Nie, and J. M. Jornet, "Terahertz Band Communication: An Old Problem Revisited and Research Directions for the Next Decade," *IEEE Transactions on Communications*, vol. 70, no. 6, 2022, doi: 10.1109/TCOMM.2022.3171800.

[2] C. Xu, Z. Ren, J. Wei, and C. Lee, "Reconfigurable terahertz metamaterials: From fundamental principles to advanced 6G applications," 2022. doi: 10.1016/j.isci.2022.103799.

[3] V. Pacheco-Peña, "Terahertz technologies and its applications," 2021. doi: 10.3390/electronics10030268.

[4] Z. Chen *et al.*, "A survey on terahertz communications," *China Communications*, vol. 16, no. 2, 2019, doi: 10.12676/j.cc.2019.02.001.

[5] R. Mahapatra, "Convergence of Wireless and Optical Network in Future Communication Network," in *Wireless Power Transfer – Recent Development, Applications and New Perspectives*, 2021. doi: 10.5772/intechopen.97293.

[6] K. Wang *et al.*, "Evolution of Short-Range Optical Wireless Communications," *Journal of Lightwave Technology*, vol. 41, no. 4, 2023, doi: 10.1109/JLT.2022.3215590.

[7] M. A. Akkaş and R. Sokullu, "Wıreless Communıcatıons Beyond 5 g: Teraherzwaves, Nano-Communıcatıons and the Internet of Bıo-Nano-Thıngs," 2022. doi: 10.1007/s11277-022-09878-6.

[8] Z. Chen *et al.*, "Terahertz Wireless Communications for 2030 and Beyond: A Cutting-Edge Frontier," *IEEE Communications Magazine*, vol. 59, no. 11, 2021, doi: 10.1109/MCOM.011.2100195.

[9] Y. Huang, Y. Shen, and J. Wang, "From Terahertz Imaging to Terahertz Wireless Communications," 2023. doi: 10.1016/j.eng.2022.06.023.

[10] D. Serghiou, M. Khalily, T. W. C. Brown, and R. Tafazolli, "Terahertz Channel Propagation Phenomena, Measurement Techniques and Modeling for 6G Wireless Communication Applications: A Survey, Open Challenges and Future Research Directions," *IEEE Communications Surveys and Tutorials*, vol. 24, no. 4, 2022, doi: 10.1109/COMST.2022.3205505.

[11] M. Božanić and S. Sinha, "Emerging transistor technologies capable of terahertz amplification: A way to re-engineer Terahertz Radar sensors," 2019. doi: 10.3390/s19112454.

[12] H. Zeng *et al.*, "A review of terahertz phase modulation from free space to guided wave integrated devices," 2022. doi: 10.1515/nanoph-2021-0623.

[13] C. Han, Y. Wu, Z. Chen, Y. Chen, and G. Wang, "THz ISAC: A Physical-Layer Perspective of Terahertz Integrated Sensing and Communication," *IEEE Communications Magazine*, vol. 62, no. 2, 2024, doi: 10.1109/MCOM.001.2200404.

[14] A. A. A. Solyman and I. A. Elhaty, "Potential key challenges for terahertz communication systems," *International Journal of Electrical and Computer Engineering*, vol. 11, no. 4, 2021, doi: 10.11591/ijece.v11i4.pp3403-3409.

[15] MOHD RASHID REDZA BIN ABDULLAH, "GaAs/AlAs ASPAT Diodes for Millimetre and Sub-Millimetre Wave Applications," Manchester, 2017.

[16] L. Liu, S. M. Rahman, Z. Jiang, W. Li, and P. Fay, "Advanced terahertz sensing and imaging systems based on integrated III-V interband tunneling devices," 2017. doi: 10.1109/JPROC.2016.2636245.

[17] I. Mehdi, J. V. Siles, C. Lee, and E. Schlecht, "THz diode technology: Status, prospects, and applications," 2017. doi: 10.1109/JPROC.2017.2650235.

[18] D. Cimbri, J. Wang, A. Al-Khalidi, and E. Wasige, "Resonant Tunneling Diodes High-Speed Terahertz Wireless Communications -A Review," 2022. doi: 10.1109/TTHZ.2022.3142965.

[19] X. Fu, Y. Liu, Q. Chen, Y. Fu, and T. J. Cui, "Applications of Terahertz Spectroscopy in the Detection and Recognition of Substances," 2022. doi: 10.3389/fphy.2022.869537.

[20] K. N. Zainul Ariffin *et al.*, "Investigations of asymmetric spacer tunnel layer diodes for high-frequency applications," *IEEE Trans Electron Devices*, vol. 65, no. 1, 2018, doi: 10.1109/TED.2017.2777803.
[21] A. E. P. Hoyos, V. Fossaluza, L. G. Esteves, and C. A. de Bragança Pereira, "Adaptive Significance Levels in Tests for Linear Regression Models: The e-Value and P-Value Cases," *Entropy*, vol. 25, no. 1, 2023, doi: 10.3390/e25010019.
[22] P. Goos and D. Meintrup, *Statistics with JMP: Hypothesis tests, ANOVA and Regression*. 2016.
[23] M. G. Tsige, A. Malcherek, and I. Baselt, "An iterative approach for deriving and solving an accurate regression equation," *Math Comput Model Dyn Syst*, vol. 30, no. 1, 2024, doi: 10.1080/13873954.2024.2313014.
[24] V. A. Barbur, D. C. Montgomery, and E. A. Peck, "Introduction to Linear Regression Analysis.," *The Statistician*, vol. 43, no. 2, 1994, doi: 10.2307/2348362.
[25] F. Tahmasebinia, R. Jiang, S. Sepasgozar, J. Wei, Y. Ding, and H. Ma, "Implementation of BIM Energy Analysis and Monte Carlo Simulation for Estimating Building Energy Performance Based on Regression Approach: A Case Study," *Buildings*, vol. 12, no. 4, 2022, doi: 10.3390/buildings12040449.
[26] L. Jerome, "Multiple linear and non-linear regression in Minitab," *MSOR Connections*, vol. 9, no. 3, 2009, doi: 10.11120/msor.2009.09030017.